Title

Outcomes of progranulin gene therapy in the retina are dependent on time and route of delivery

Authors

Zin, Emilia A
Han, Daisy
Tran, Jennifer
et al.

Publication Date

2021-09-01

DOI

10.1016/j.omtm.2021.05.009

Peer reviewed

Molecular Therapy
Methods & Clinical Development
Original Article

Outcomes of progranulin gene therapy in the retina are dependent on time and route of delivery

Emilia A. Zin,[1] Daisy Han,[2] Jennifer Tran,[3] Nikolas Morisson-Welch,[4] Meike Visel,[4] Mervi Kuronen,[4] and John G. Flannery[1,3,4]

[1]Vision Science Group, School of Optometry, UC Berkeley, Berkeley, CA 94720, USA; [2]Department of Integrative Biology, UC Berkeley, Berkeley, CA 94720, USA; [3]School of Optometry, UC Berkeley, Berkeley, CA 94720, USA; [4]Helen Wills Neuroscience Institute, UC Berkeley, Berkeley, CA 94720, USA

Neuronal ceroid lipofuscinosis (NCL) is a family of neurodegenerative diseases caused by mutations to genes related to lysosomal function. One variant, CNL11, is caused by mutations to the gene encoding the protein progranulin, which regulates neuronal lysosomal function. Absence of progranulin causes cerebellar atrophy, seizures, dementia, and vision loss. As progranulin gene therapies targeting the brain are developed, it is advantageous to focus on the retina, as its characteristics are beneficial for gene therapy development: the retina is easily visible through direct imaging, can be assessed through quantitative methods *in vivo*, and requires smaller amounts of adeno-associated virus (AAV). In this study we characterize the retinal degeneration in a progranulin knockout mouse model of CLN11 and study the effects of gene replacement at different time points. Mice heterologously expressing progranulin showed a reduction in lipofuscin deposits and microglia infiltration. While mice that receive systemic AAV92YF-scCAG-PGRN at post-natal day 3 or 4 show a reduction in retina thinning, mice injected intravitreally at months 1 and 6 with AAV2.7m8-scCAG-PGRN exhibit no improvement, and mice injected at 12 months of age have thinner retinas than do their controls. Thus, delivery of progranulin proves to be time sensitive and dependent on route of administration, requiring early delivery for optimal therapeutic benefit.

INTRODUCTION

Neuronal ceroid lipofuscinosis (NCL), or Batten disease, is a family of disorders characterized by the accumulation of autofluorescent lipofuscin in neurons.[1] Clinically, NCL patients frequently report seizures, progressive vision loss, and motor and cognitive decline.[1] There are at least 14 different variants of NCL, each caused by mutations to different genes. These variants are labeled sequentially: CLN1, CLN2, CLN3, and so forth.[2,3] CLN11, identified in 2012 in a pair of Italian siblings, is caused by biallelic mutations in the progranulin *GRN* (or *PGRN*) gene.[4] These patients present vision loss, seizures, ataxia, and cognitive decline.[5] Interestingly, single-allele mutations in *GRN* may also cause frontotemporal dementia (FTD).[6,7]

Progranulin is an 88-kDa glycoprotein expressed in multiple cell types.[8] The full protein is composed of seven and a half tandem repeats of cysteine-rich sequences. Progranulin is mainly secreted by microglia and endocytosed by neurons through sortilin receptors, then shuttled to the endolysosome and early lysosome, where it is cleaved into the seven separate granulins by three different lysosomal proteases: cathepsins B, D, and L.[9–11]

Progranulin directly or indirectly affects lysosomal biogenesis and autophagy through transcriptional regulation. Transcriptional activation of lysosomal genes by the coordinated lysosomal expression and regulation (CLEAR) sequence, and subsequent lysosomal upregulation, seems to be related to protein aggregation and mislocalization.[12] This leads to one of the hallmarks of NCL: accumulation of lipofuscin, an autofluorescent granule deposit composed of proteins, lipids, sugars, and metals.[13] Lipofuscin naturally accumulates in several tissues with age, but mitochondrial or lysosomal damage can increase lipofuscin deposits. Since all NCLs present some form of lysosomal damage, accumulation of lipofuscin represents a hallmark of the disease, which also applies to CLN11.[14] As such, lipofuscin accumulation can be used as a biomarker for NCL therapies (M. Ward et al., 2012, Am. Acad. Neurol., conference).

Most types of NCL are shown by animal models that replicate disease progression. For CLN11 there are several mouse models in which *GRN* was knocked out by different methods.[15,16] The homozygous $PGRN^{-/-}$ mouse line used in this study shows slow neurodegeneration, with loss of neurons by 12 months of age, an increase in microglial activation, and mild behavioral alterations, but no seizures.[16,17] Several studies analyzed neuronal degeneration in the mouse brain, but very few reported on retinal degeneration progression, which is addressed in this study.[18–20]

Received 5 March 2021; accepted 19 May 2021;
https://doi.org/10.1016/j.omtm.2021.05.009.

Correspondence: John G. Flannery, Vision Science Group, School of Optometry, 112 Barker Hall, UC Berkeley, Berkeley, CA 94720, USA.
E-mail: flannery@berkeley.edu

Gene replacement is an excellent strategy for NCL therapy; almost all NCLs are autosomal recessive, so the delivery of a functional copy of the mutated gene should theoretically restore cellular function. Delivery of a transgene cassette can be carried out with a viral vector such as the adeno-associated virus (AAV). The transgene cassette can carry a cell-specific promoter or a ubiquitous promoter. Examples of ubiquitous promoters include the human cytomegalovirus (CMV) promoter or the synthetic CAG promoter, which is composed of a CMV enhancer fused to the chicken β-actin promoter.

There are several promising NCL gene therapies with AAV currently under preclinical and clinical development (ClinicalTrials.gov: NCT03770572 and NCT04273243). Preclinical mouse studies include a gene therapy for CLN8, where expression of the *CLN8* gene, delivered via an AAV9 capsid by an intracerebroventricular injection, prolongs the CLN8 mouse model's lifespan and restores its normal behavior.[21] Similarly, $CLN6^{nclf}$ mice show a reduction in cell death after intravitreal delivery of *CLN6* to bipolar cells through the AAV2.7m8 (7m8) capsid.[22] Two studies have tackled gene therapy in $PGRN^{-/-}$ mice: one reports improvement in lysosomal function after bilateral stereotaxic injections of rAAV2-CBA-PGRN in the medial prefrontal cortex (mPFC), and the other describes hippocampal atrophy due to T-cell toxicity after unilateral stereotaxic posterior right lateral ventricle injections of rAAV4-CAG-PGRN or rAAV9-CMV-PGRN.[23,24] Neither looked at the effects of PGRN gene therapy in the retina.

A retina-focused study could provide critical insights into the effects of a progranulin gene therapy. Not only is the retina a window to the brain, but electrophysiology and direct imaging easily monitor it over time. Furthermore, most patients with biallelic *GRN* mutations report vision loss and would likely require viral delivery targeted to the retina itself. Given the GRN-FTD clinical trial under way, as well as the conflicting gene therapy results already published that reveal lysosomal function improvement but hippocampal atrophy, a gene therapy study targeting progranulin to the retina would provide further data on treatment efficacy over time (ClinicalTrials.gov: NCT04408625).

We hypothesized that delivery of either mouse PGRN (mPGRN) or human PGRN (hPGRN) to all cell layers of the retina via AAV vectors would slow down or prevent degeneration. We also hypothesized that early delivery would be more effective at stalling or slowing neurodegeneration. We selected the 7m8 and AAV9.2YF capsids to test these hypotheses. 7m8 was selected as an engineered capsid capable of reaching all cell layers in the retina when injected from the vitreous in adult mice.[25] As AAV9 can cross the blood-retina and blood-brain barriers in mice until 7 days of age, it seemed an appropriate choice for intravenous deliveries in mice pups between post-natal days 3 and 4 (P3 and P4), when direct retinal delivery is challenging due to eye size and closed eyelids.[26] The included mutations on the AAV9 capsid, i.e., Y446F and Y731F (AAV9.2YF), improve gene transfer by inhibiting the proteasomal degradation of the AAV capsid. In both constructs, we used the ubiquitous and synthetic promoter CAG in a self-complementary (sc) plasmid. Both mPGRN and hPGRN were selected as transgenes; hPGRN was chosen to observe any toxicity effects in the murine model, as well as to serve as a point of comparison to the study conducted by Amado et al.[24] Animals received intravitreal injections with 7m8-scCAG-PGRN at 1, 6, and 12 months of age. Mice treated at 1 and 6 months were euthanized at 12 months of age, and mice treated at 12 months were euthanized at 18 months of age. Mice that received AAV92YF-scCAG-PGRN through a tail vein injection at P3 or P4 were euthanized at 12 months of age.

RESULTS

$PGRN^{-/-}$ model characterization

$PGRN^{-/-}$ mice have been used in several studies to understand the development of NCL and FTD, and although pathological degeneration in the brain has been studied extensively, the time course and pathologic changes in the retinal degeneration is less well understood. Previous studies have reported retinal thinning by 12 and 18 months of age but do not report on earlier time points.[19] Therefore, we compared retinas of $PGRN^{-/-}$ and C57BL/6J mice over time (Figure 1). To explore retinal thinning, overall retinal (inner-limiting membrane to retinal pigment epithelium [RPE]) and photoreceptor layer (outer nuclear layer [ONL] to RPE) thicknesses were measured by optical coherence tomography (OCT) imaging at months 1, 5, 12, and 18 (Figures 1A–1D, respectively). $PGRN^{-/-}$ photoreceptor layers were significantly thinner than those of C57BL/6J retinas at 1, 5, 12, and 18 months of age (Figures 1A–1D). However, statistically significant overall retinal thinning of $PGRN^{-/-}$ retinas only occurred at 12 and 18 months of age (Figures 1C and 1D). Total retina thickness decreased between 7.8% and 14.4% at 12 months, and between 10.4% and 16.6% at 18 months of age. Photoreceptor layer thickness decreased between 14.3% and 24.5% at 12 months, and between 17.8% and 30.4% at 18 months of age.

Electroretinograms (ERGs) reflect the electrical activity of retinal neurons and glial cells generated in response to light. A- and B-wave amplitude data derived from scotopic and photopic ERGs from C57BL/6J and $PGRN^{-/-}$ mice at 1, 3, 7, 9 and 12 months of age are shown in Figure S1. Significant strain-dependent differences in scotopic A-wave amplitudes are seen at 7 and 9 months of age (Figure S1A).

A previous study by Ward et al.[27] reported increases in retinal lipofuscin deposits at months 1.5, 3, 6, 12, and 18. To replicate their findings, retinal flat mounts were imaged under fluorescence microscopy. Lipofuscin was visible principally in $PGRN^{-/-}$ retinas (Figure 1E). $PGRN^{-/-}$ retinas showed a trend in lipofuscin increase when compared to C57BL/6J retinas at months 1, 3, and 9. The difference became statistically significant at months 12 and 18.

We compared the endogenous expression of PGRN in C57BL/6J mice to expression driven by 7m8-scCAG-mPGRN (Figures 1F–1H). At 1 month of age, 7m8-scCAG-mPGRN was intravitreally injected in the right eye (OD) and sterile phosphate-buffered saline (PBS) in the left eye (OS) of $PGRN^{-/-}$ mice. Animals were euthanized at

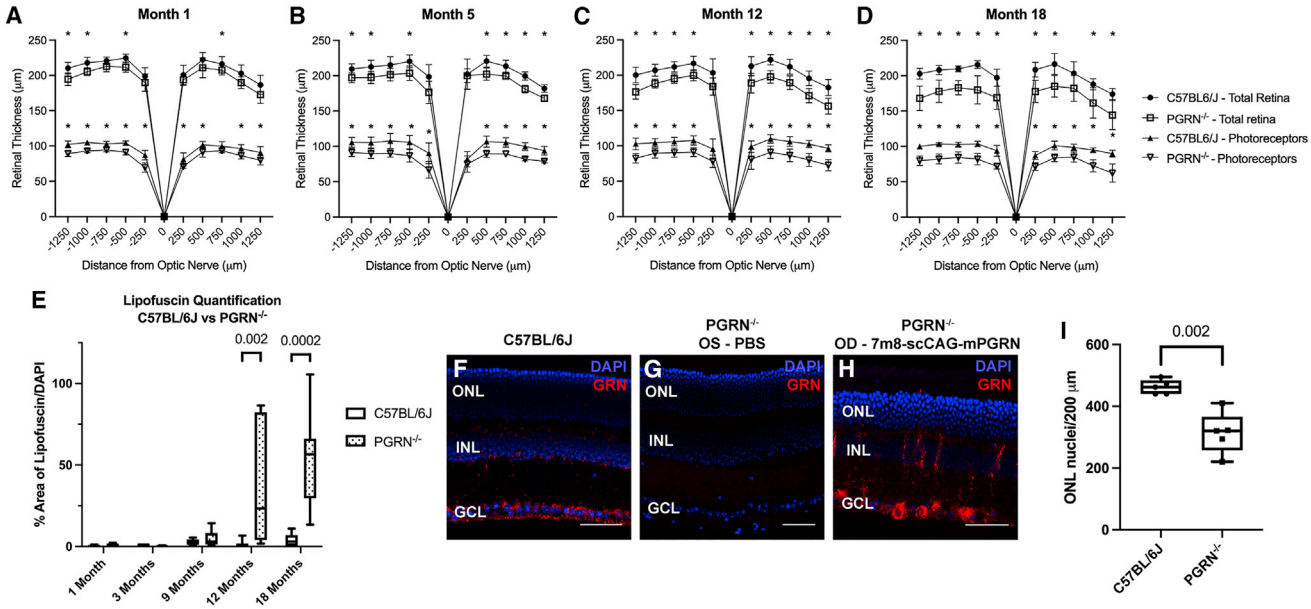

Figure 1. Retinal degeneration in PGRN$^{-/-}$ mice over time

Optical coherence tomography (OCT) measurements in superior (−250 to −1,250 μm from the optic nerve) and inferior (250 to 1,250 μm from the optic nerve) retinas are shown. Total retina thickness was measured from the ILM to the RPE (upper curves: ●, C57BL/6J; □, PGRN$^{-/-}$), and photoreceptor layer thickness was measured from the ONL to the RPE (lower curves: ▲, C57BL/6J; ▽, PGRN$^{-/-}$). (A–D) Month 1 (A), month 5 (B), month 12 (C), and month 18 (D) were recorded. Error bars represent ± standard deviation, and a ● or ▲ stands for mean values for retinal thickness of n = 7 animals per group for C57BL/6J at months 1 and 18, n = 6 for month 5, and n = 9 for month 12. A □ or ▽ stands for mean values for retinal thickness for PGRN$^{-/-}$ mice of n = 5 animals per group at months 1, 5, and 18, and n = 10 for month 12. A two-way ANOVA with multiple comparisons was performed for each month between mouse strains, with Geisser-Greenhouse correction and a Fisher's LSD test. *p < 0.05 (A–D). (E) Lipofuscin was mainly found in PGRN$^{-/-}$ retinas and quantified by measuring total area covered by lipofuscin in flat mounts over total area covered by nuclei in DAPI at different time points. In the box-and-whiskers plot, boxes show interquartile range (25%–75%), whiskers represent minimum and maximum values, and horizontal lines represent median values of six animals at months 3 and 9, and eight animals at months 1, 12, and 18. A Mann-Whitney statistical test between mouse strains at different time points was used; p values are indicated. n = 6 or n = 8 per group. (F–H) Immunohistochemistry for PGRN in either C57BL/6J retina (F), PGRN$^{-/-}$ OS retina with PBS injection (G), or PGRN$^{-/-}$ OD retina expressing mPGRN through 7m8-scCAG-mPGRN intravitreal injection (H). DAPI staining nuclei (blue) and PGRN (red) are shown. (I) Quantification of photoreceptor nuclei in C57BL/6J and PGRN$^{-/-}$ retinas, where nuclei in the ONL were measured along 200 μm adjacent to the optic nerve. In the box-and-whiskers plot, boxes show interquartile range (25%–75%), whiskers represent minimum and maximum values, and horizontal lines represent median values of five animals/group. Inter-strain difference was statistically significant (Mann-Whitney test, p = 0.0079). Scale bars, 50 μm.

9 months for tissue collection. Endogenous PGRN expression in C57BL/6J mice was primarily seen in the ganglion cell layer (GCL) and inner nuclear layer (INL), with some expression in the ONL (Figure 1F). PGRN$^{-/-}$ eyes injected with PBS showed no PGRN expression (Figure 1G). Retinas injected with 7m8-scCAG-mPGRN transduced mouse PGRN in the GCL, INL, Müller glia, and occasional photoreceptors (Figure 1H), confirming that PGRN$^{-/-}$ retinas could widely express PGRN through a ubiquitous promoter at 8 months post-injection.

Intravitreal injections at 1 and 6 months of age

Mice intravitreally injected at 1 and 6 months of age with either 7m8-scCAG-mPGRN or 7m8-scCAG-hPGRN were euthanized at 12 months, enucleated, and retinal tissue was collected for processing. Immunohistochemistry for mPGRN and hPGRN showed an overall increase in PGRN expression in PGRN$^{-/-}$ mice injected at 6 months of age (Figure 2). PGRN was highly expressed in the GCL (Figures 2A, 2E, and 2I) and also found in photoreceptors and Müller glia (Figure 2A) and bipolar cells (Figure 2I). Microglia infiltrated the INL in all panels (arrowheads, Figures 2D, 2G, 2H, 2K, and 2L), but not in Figure 2C. Therefore, microglial infiltration occurred in all contralateral control retinas, but not in one expressing PGRN (Figure 2C).

PGRN$^{-/-}$ retinas expressing mPGRN showed a remarkable reduction in lipofuscin deposits (Figure 2S). Lipofuscin is visible through autofluorescence in retina cross-sections (Figures 2M and 2P). Animals that received intravitreal injections of mPGRN at 6 months of age showed a significant reduction in lipofuscin deposits when compared to contralateral control eyes injected with PBS (Figure 2S). A significant reduction was not detected in animals injected at 1 month (Figure 2Q). Alternatively, animals transducing human PGRN showed a similar but non-significant reduction in retinal lipofuscin (Figure 2R).

There were no significant differences in retina thickness between treated and control eyes as quantified by retinal layer measurements

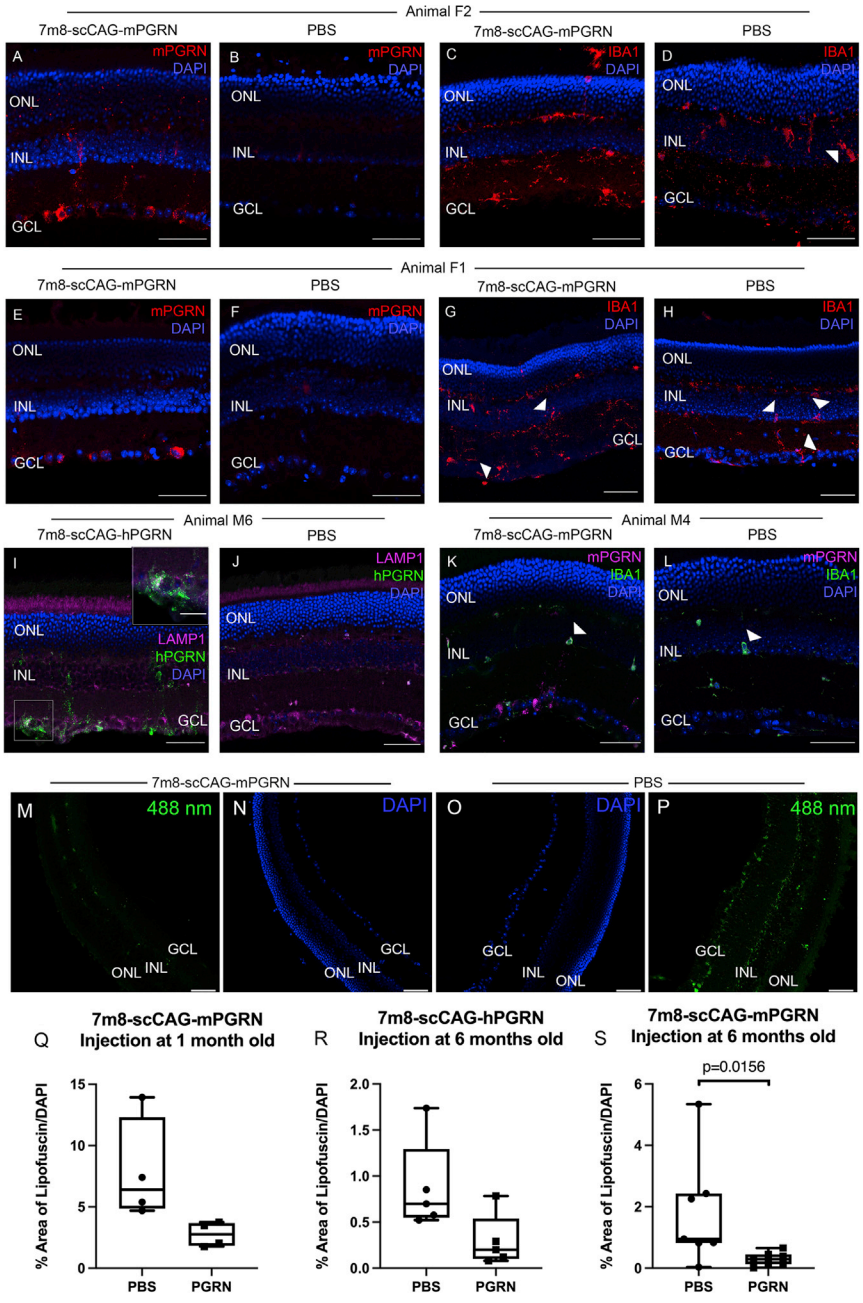

Figure 2. Immunohistochemistry on retinas of PGRN$^{-/-}$ mice treated at 6 months of age and injected with either 7m8-scCAG-mPGRN, 7m8-scCAG-hPGRN, or PBS

(A, C, E, G, and K) Mice injected with 7m8-scCAG-mPGRN. (I) Mice injected with7m8-scCAG-hPGRN. (B, D, F, H, J, and L) Mice injected with PBS. (A, E, and I) Mice show PGRN expression mainly in RGCs, but also in bipolar cells, Müller cells, and photoreceptors. (D, G, H, K, and L) IBA1 shows microglia migrating to the INL and GCL (arrowheads) in all sections except (C). (I) LAMP1 indicates little overlap between PGRN and lysosomes, except for some puncta (inset). (K) Similarly, there is little overlap between PGRN and microglia. DAPI (blue), mPGRN (red), hPGRN (green), IBA1 (red or green, as indicated). (M–P) Lipofuscin can be seen autofluorescing in PGRN$^{-/-}$ retina cross-sections under 488-nm laser. (M) Retinas expressing mPGRN visibly present a reduced amount and intensity of lipofuscin deposits. (Q–S) Quantification of lipofuscin deposits as the percentage of overall lipofuscin over total DAPI shows statistically significant reduction of lipofuscin in retinas transducing mPGRN at 6 months (S) but not at 1 month of age (Q) or expressing hPGRN at 6 months of age (R). In box-and-whiskers plot, boxes show interquartile range (25%–75%), whiskers represent minimum and maximum values, and horizontal lines represent median values of four animals (Q), five animals (R), and seven animals (S). (S) Wilcoxon signed rank test between eyes transducing progranulin and contralateral control eyes; p = 0.0156. Lipofuscin (green) and DAPI (blue). Scale bars: 50 μm for all panels, 20 μm for the inset.

by OCT imaging (Figures 3A–3C). Retinal thickness was measured at 12 months and there were no significant differences between treated and contralateral control retinas. There were only three points in the retinas of mice injected at 6 months of age and transducing mPGRN that were an exception, showing statistically significant differences. There was a trend, albeit non-significant, toward reduction in total retina and photoreceptor layer thicknesses in treated versus control eyes in animals injected at 1 month (Figure 3A), as well as in total retina thickness of animals injected at 6 months of age (Figures 3B and 3C). Counting ONL nuclei corroborated these findings (Figures 3D–3F). There was a significant reduction in the amount of photoreceptor nuclei in the retinas of animals injected with 7m8-scCAG-mPGRN at 6 months (Figure 3F), but not in the retinas of animals injected at 1 month (Figure 3D), or in retinas of animals injected with hPGRN at 6 months of age (Figure 3E).

Intravitreal injections at 12 months of age

Mice intravitreally injected at 12 months of age with 7m8-scCAG-mPGRN were euthanized at 18 months of age and retinas were collected for processing. Immunohistochemistry demonstrated the presence of transduced mPGRN in eyes receiving 7m8-scCAG-mPGRN, but not in PBS-injected contralateral controls (Figures 4A–4C, 4E, and 4F). PGRN expression was highest in retinal ganglion cells (RGCs) and expressed to a lesser extent in bipolar cells, Müller glia, and photoreceptors (Figures 4A, 4C, and 4E). There was large variability in expression patterns, despite being injected with the same viral stock (2 μL at 3.97E+13 vector genomes [vg]/mL) and by the same researcher. In Figure 2, IBA1 labeling showed microglia infiltrating mainly the INL, but also the GCL and ONL, in both treated and control retinas. However, treated retinas showed fewer

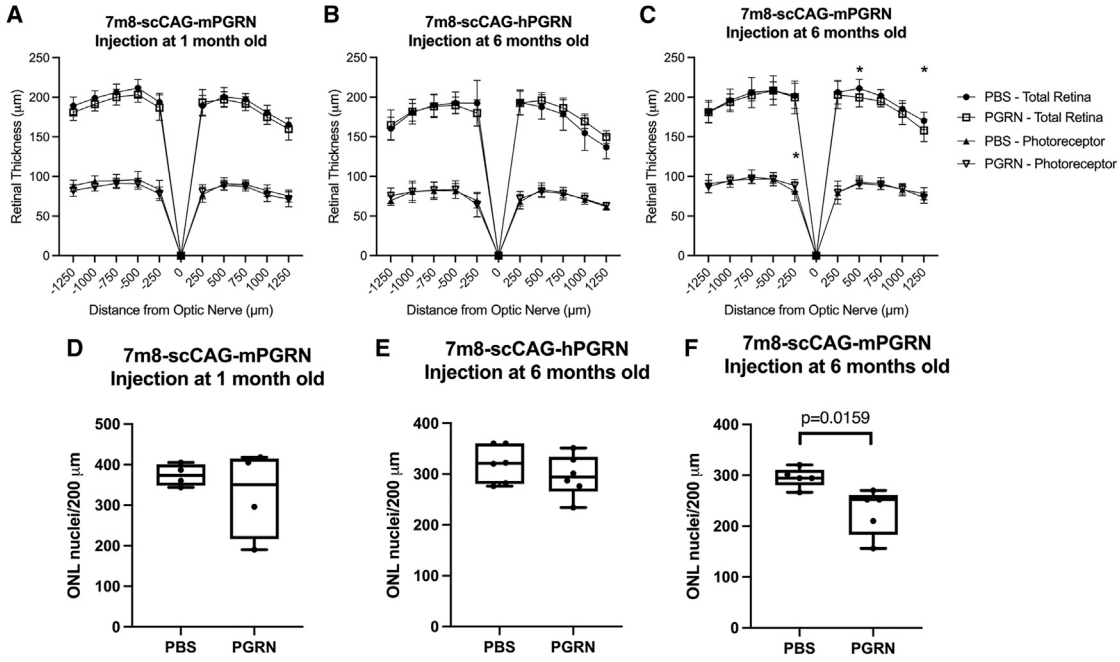

Figure 3. OCT measurements and ONL quantification in animals injected at 1 and 6 months of age

OCT quantification in superior (−250 to −1,250 µm from the optic nerve) and inferior (250 to 1,250 µm from the optic nerve) PGRN$^{-/-}$ retinas is shown. (A–C) Total retina thickness was measured from the ILM to the RPE, and photoreceptor layer thickness was measured from the ONL to the RPE in PGRN$^{-/-}$ mice intravitreally injected with 7m8-scCAG-mPGRN at 1 month (A), 7m8-scCAG-hPGRN at 6 months (B), or 7m8-scCAG-mPGRN at 6 months of age (C). Curves compare total thickness of retinas expressing PGRN (□) and control retinas that received PBS (●), or photoreceptor layer thickness of the same retinas expressing PGRN$^{-/-}$ (▽), and control retinas that received PBS (▲). Error bars represent ± standard deviation, and circles or squares represent mean values for retinal thickness for 10 animals per group in (A) and (C), and 8 animals per group in (B). A two-way ANOVA with multiple comparisons was performed for each experimental group, with a Geisser-Greenhouse correction and Fisher's LSD test. *p < 0.05. (D–F) ONL nuclei in retina cross-sections were quantified over 200-µm sections adjacent to the optic nerve in mice injected at 1 month of age (D), 6 months of age and expressing hPGRN (E), or 6 months of age and expressing mPGRN (F). In the box-and-whiskers plot, boxes show interquartile range (25%–75%), whiskers represent minimum and maximum values, and horizontal lines represent median values of five animals. For the Mann-Whitney statistical test between control and treated retinas, p = 0.0159; n = 4 (D), n = 6 (E), and n = 5 (F).

microglia infiltration events than did control retinas (arrows, Figures 4G and 4H). Interestingly, the retinas that expressed mPGRN were thinner than their contralateral controls (Figure 4I). This statistically significant difference was seen in total retinal thickness and photoreceptor layer thickness of the inferior retina. Similarly to the previous cohort of animals injected with 7m8-scCAG-mPGRN at 6 months (Figure 2), PGRN$^{-/-}$ retinas that expressed virally delivered PGRN showed a dramatic and statistically significant decrease in lipofuscin deposits in comparison to contralateral controls (Figure 4J). The trend in ONL nuclei numbers was also comparable to previous results in animals injected at 1 and 6 months, whose retinas that expressed PGRN showed a non-statistically significant trend of reduction in photoreceptor nuclei number in comparison to PBS controls (Figure 4K).

Intravenous injections at P3–P4

Mouse pups injected intravenously at P3 or P4 were euthanized at 12 months of age, perfused, and enucleated. Immunohistochemistry for mPGRN and hPGRN showed an increase in PGRN expression in PGRN$^{-/-}$ mice injected with AAV9.2YF-scCAG-mPGRN and AAV9.2YF-scCAG-hPGRN, respectively (Figures 5A and 5C). Progranulin was mainly observed in RGCs (Figure 5A), although it was also found in bipolar cells and Müller glia (Figure 5C). Retinas from naive control animals showed no PGRN expression (Figure 5B).

OCT imaging revealed a significant increase in total retina thickness of mice transducing mPGRN, and a significant overall increase in the photoreceptor layer thickness, when compared to naive controls (Figure 5D). Curiously, these trends are opposite to those reported in animals injected at 1, 6, and 12 months of age, which showed reductions in total retinal thickness in the presence of PGRN expression (Figures 3 and 4).

However, we observed a significant reduction in lipofuscin deposits in these mice as well, indicating that despite the difference in retinal thickness, PGRN still prevented lipofuscin accumulation (Figure 5E). There was a trend in detecting more photoreceptor nuclei in mice injected with AAV9.2YF-scCAG-mPGRN than in control animals (Figure 5F). Although not statistically significant, this trend goes against

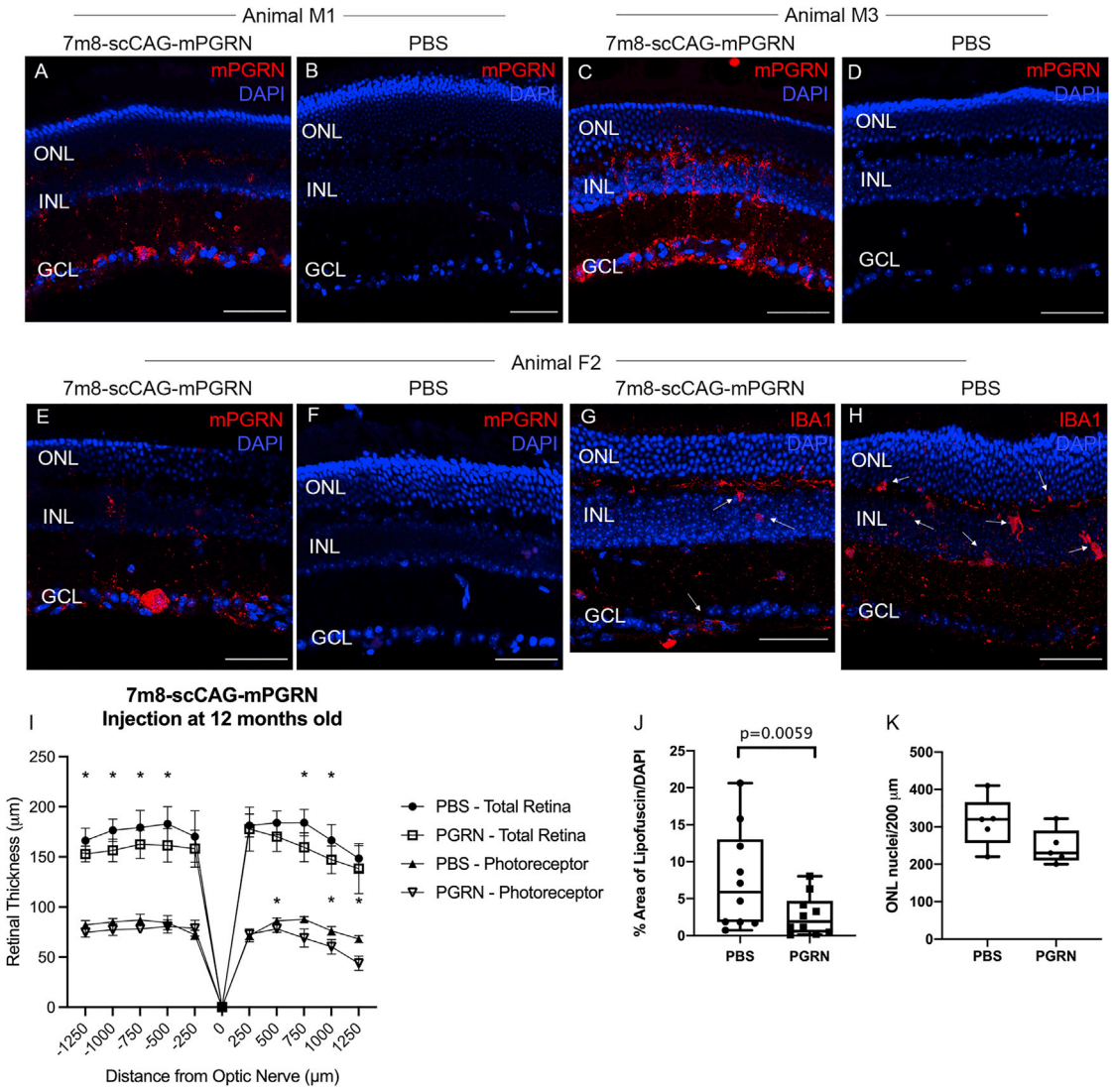

Figure 4. Immunohistochemistry on retinas of PGRN$^{-/-}$ mice injected at 12 months of age with 7m8-scCAG-mPGRN or PBS

(A, C, E, and G) Mice injected with scCAG-mPGRN. (B, D, F, and H) Mice injected with PBS. (A, C, and E) Mice show mPGRN expression mainly in RGCs, but also in bipolar cells, Müller cells, and photoreceptors. (G and H) IBA1, a microglia marker, shows microglia migrating to the INL and GCL (arrows) in both treated and control retinas. (H) However, microglia seem to be infiltrating nuclear layers more frequently in the control mouse. DAPI (blue), mPGRN (red), IBA1 (red). Scale bars, 50 µm. (I) OCT measurements for superior (−250 to −1,250 µm from the optic nerve) and inferior (250 to 1,250 µm from the optic nerve) PGRN$^{-/-}$ retinas. Total retina thickness was measured from the ILM to the RPE, and photoreceptor layer thickness was measured from the ONL to the RPE in PGRN$^{-/-}$ mice, showing retinal thinning in mice transducing PGRN. Curves compare total thickness of retinas expressing PGRN (□) and control retinas that received PBS (●), or photoreceptor layer thickness of the same retinas expressing PGRN (▽) and control retinas that received PBS (▲). Error bars represent ± standard deviation, and circles, squares, or triangles represent mean values for retinal thickness of eight animals per group. A two-way ANOVA with multiple comparisons was performed between experimental groups, with a Geisser-Greenhouse correction and Fisher's LSD test. *$p < 0.05$. (J) Quantification of lipofuscin deposits as the percentage of overall lipofuscin over total DAPI shows statistically significant reduction in lipofuscin in retinas transducing mPGRN. (K) ONL nuclei in retina cross-sections were quantified along 200-µm sections adjacent to the optic nerve for treated and control retinas. In the box-and-whiskers plot, boxes show interquartile range (25%–75%), whiskers represent minimum and maximum values, and horizontal lines represent median values. For the Wilcoxon signed rank test between control and treated retinas, $p = 0.0059$ for lipofuscin measurements (J) and $p = 0.125$ (ns [not significant]) for density of ONL nuclei (K).

the data in Figures 2 and 4, where mice with intravitreal injection of 7m8-scCAG-PGRN showed a trend of photoreceptor loss and retina thinning.

Moreover, the hippocampi of these mice exhibited a striking difference in lipofuscin deposits (Figure S2). Brain sections of both injected and naive control mice were compared by imaging the dentate gyrus

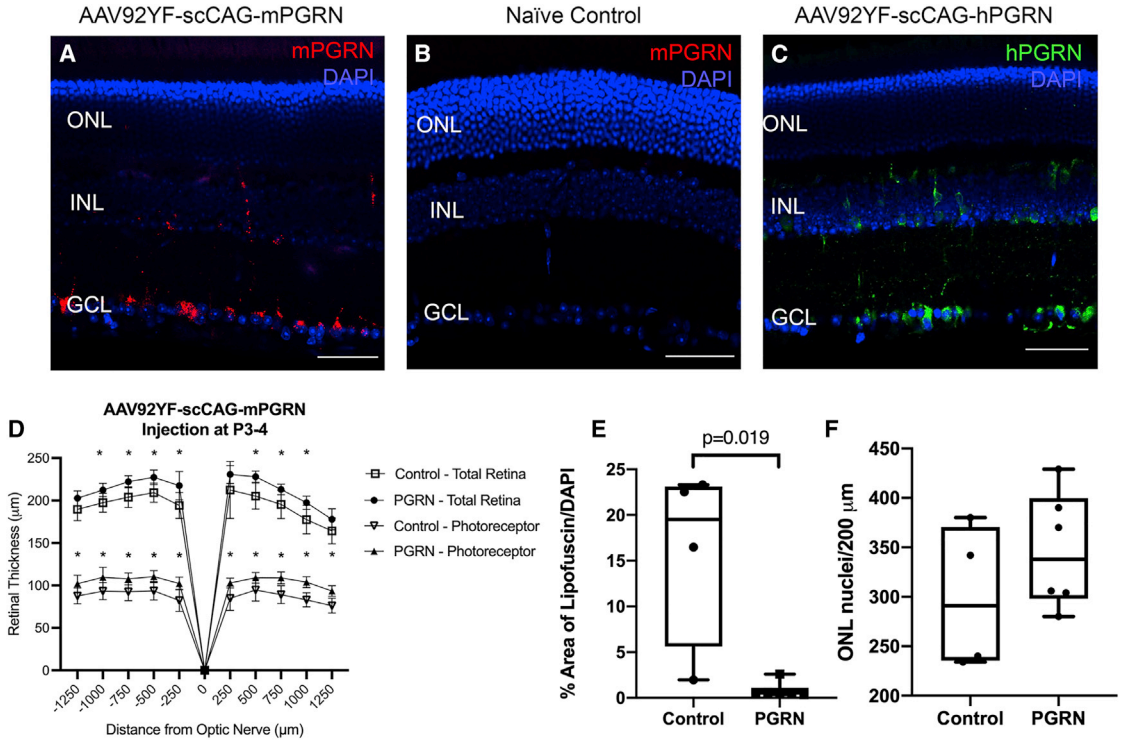

Figure 5. PGRN expression, ONL nuclei, and lipofuscin area quantification

(A–C) Immunohistochemistry for PGRN in retinas of mice intravenously injected with AAV92YF-scCAG-mPGRN (A), AAV92YF-scCAG-hPGRN (C), or not injected (B). DAPI (blue), mPGRN (red), hPGRN (green). Scale bars, 50 µm. (D) OCT measurements for superior (−250 to −1,250 µm from the optic nerve) and inferior (250 to 1,250 µm from the optic nerve) PGRN$^{-/-}$ retinas. Total retina thickness was measured at 12 months of age, from the ILM to the RPE, and photoreceptor layer thickness was measured from the ONL to the RPE in PGRN$^{-/-}$ mice intravenously injected with AAV92YF-scCAG-mPGRN at post-natal day 3 (P3) or 4 (P4). Curves compare total thickness of retinas expressing PGRN (□) and naive control retinas (●), or photoreceptor layer thickness of the same retinas expressing PGRN (▽) and control retinas (▲). Error bars represent ± standard deviation, and circles or squares represent mean values for retinal thickness of six animals per group. A two-way ANOVA with multiple comparisons was performed for each experimental group, with a Geisser-Greenhouse correction and Fisher's LSD test. *p < 0.05. (E) Quantification of lipofuscin deposits as the percentage of overall lipofuscin over total DAPI shows statistically significant reduction in lipofuscin in retinas transducing mPGRN. (F) ONL nuclei in retina cross-sections were quantified over 200-µm sections adjacent to the optic nerve in treated and control retinas. In the box-and-whiskers plot, boxes show interquartile range (25%–75%), whiskers represent minimum and maximum values, and horizontal lines represent median values. For the Mann-Whitney statistical test between control and treated retinas, p = 0.352 (ns) (F) and p = 0.019 (E) (n = 4 [PBS] and n = 6 [PGRN]).

(DG), field CA1 and third ventricle (V3). Lipofuscin reduction in four mice expressing PGRN corroborated the ability of progranulin to reduce lipofuscin accumulation, when compared to four naive controls (Figure S2E).

DISCUSSION

The hypothesis driving the current study was that the delivery of progranulin to PGRN$^{-/-}$ mice would prevent or slow down retinal degeneration, with earlier intravitreal injections resulting in greater therapeutic effect. However, we observed something altogether more complex: gene delivery in 1- and 6-month-old mice did not halt or prevent retinal degeneration. Furthermore, delivery to 12-month-old animals led to further tissue loss. The observed consistent reduction in lipofuscin deposits and microglia infiltration indicates improvement. Nevertheless, delivery to mouse pups elicited an improvement in both retinal thickness and accumulation of lipofuscin. A summary is shown in Table 1.

Accumulation of autofluorescent lipofuscin represents a reported indicator of NCL disease, both in the brain and retina, and it can be detected by fluorescence microscopy.[14] It was a quantifiable biomarker for CLN11 and other NCL models in earlier studies. Therefore, establishing the levels of lipofuscin deposits in wild-type and PGRN$^{-/-}$ retinas over time was important. Initial experiments characterizing the model showed that lipofuscin can be used as a reliable biomarker of the disease process, and Ward et al.[27] reported that a lipofuscinosis increase in PGRN$^{-/-}$ mice is statistically significant as early as 1.5 months of age in comparison to C57BL/6J controls. In this study, however, deposits were significantly increased in PGRN$^{-/-}$ mice only at 12 and 18 months of age when compared to C57BL/6J controls (Figure 1E). The difference could be explained by the quantification methods: Ward et al. quantified lipofuscin puncta per mm^2, while in this study the area of lipofuscin autofluorescence was quantified and normalized to DAPI. Our OCT results showed months 12 and 18 as reliable endpoints for retinal thickness assessment due to

Table 1. Summary of outcome measures

Age at injection	Age at euthanasia	Total retinal thickness (OCT)	Photoreceptor layer thickness (OCT)	Lipofuscin	ONL nuclei	Microgliosis
1 month	12 months	–	–	–	–	N/A
6 months	12 months	–	–	↓	↓	↓
12 months	18 months	↓	↓ (inferior)	↓	–	↓
P3–P4	12 months	↑	↑	↓	–	N/A

Total retinal thickness, photoreceptor layer thickness, lipofuscin accumulation, ONL nuclei numbers, and microgliosis of retinas transducing progranulin, as compared to respective controls. Symbols: –, no change; ↓, decrease in comparison to controls; ↑, increase in comparison to controls. N/A, not applicable.

significant differences between C57BL/6J and PGRN$^{-/-}$ mice (Figures 1A–1D). Similarly, quantifying nuclei in the ONL showed a statistically significant reduction in photoreceptors in PGRN$^{-/-}$ retinas when compared to C57BL/6J mice at 12 months of age (Figure 1I). Retinal degeneration is slow in this model, and there is no complete loss of photoreceptors. Therefore, scotopic or photopic ERG results showed no statistically significant difference between mouse strains, except for two time points (Figure S1). These response patterns were consistent with histological data that showed relatively little photoreceptor cell death in PGRN$^{-/-}$ mice. A statistically significant reduction in the overall number of photoreceptors occurred by 12 months, but even by 18 months the mice still retained functional photoreceptors. Therefore, ERG comparisons were not considered a sensitive indicator of disease progression for use in evaluating therapeutic efficacy. Rather, ERG results served to confirm the results seen in OCT imaging on an electrophysiological basis.

The 7m8 capsid was chosen for intravitreal injections in adult mice due to its ability to infect cells in all layers of the retina from the vitreous. Since loss of progranulin leads to loss of photoreceptors and thinning of the inner limiting membrane (ILM) and GCL in human patients and knockout mice, it was preferable to target all retinal layers.[20] Furthermore, similar to the AAV2 and AAV5 vectors, intravitreal delivery of 7m8 causes a humoral immune response that prevents further transduction after re-administration, but it does not cause tissue damage owing to the immune response in mice.[25] The AAV9.2YF capsid was chosen for intravenous delivery in mouse pups because of its ability to cross the blood-retina and blood-brain barriers in early post-natal days.[26,28] Therefore, the viral construct was systemically delivered to both brain and retina tissues. Furthermore, intravitreal delivery would not be possible at an early post-natal time point.

Reduction in lipofuscin deposits was a consistent trend in PGRN$^{-/-}$ mice that received either 7m8-scCAG-PGRN or AAV9.2YF-scCAG-PGRN (Figures 2Q–2S, 4J, and 5E). We expected mice expressing PGRN from young adulthood to show robust reduction in overall lipofuscin accumulation, but this was not the case. Mice injected at P3–P4, 6 months of age, or 12 months of age showed the most dramatic reductions in lipofuscin accumulation. Interestingly, mice intravenously injected at P3–P4 presented similar retinal reductions in lipofuscin to those of mice intravitreously injected at 6 months of age ($p = 0.0190$ and $p = 0.0156$, respectively), while mice treated at 12 months showed the most dramatic reduction among all four groups ($p = 0.0059$). Importantly, however, note that mice treated at 12 months were euthanized at 18 months of age, 6 months later than animals in the other groups. This extended period for accumulation of lipofuscin deposits might have exaggerated the differences between treated and control eyes. Finally, the treatment also reduced lipofuscin accumulation in the hippocampi of mice intravenously injected with AAV9.2YF-scCAG-mPGRN (Figure S2).

The retinal thickness data obtained by OCT imaging tell a different story. Here, we can see the critical role that OCT imaging can play in allowing quantification of retinal changes in live animals at different time points; additionally, it circumvents the problem of histological artifacts during measurements. While cohorts treated at 1 and 6 months of age showed a slight trend in retinal thinning when they expressed progranulin in comparison to contralateral control eyes (Figures 3A–3C), animals injected at 12 months of age exhibited statistically significant reductions in retinal thickness (Figure 4I). Once again it must be pointed out that the first two groups treated at 1 and 6 months were euthanized at 12 months of age, while the third cohort was euthanized at 18 months of age. Thus, it is possible that the more exaggerated changes in the latter group were a product of further aging rather than a reflection of the age of treatment. Additional experiments are needed to distinguish between these possibilities.

The only group to bear out the proposed hypothesis that transducing PGRN would slow retinal degeneration was that injected at P3–P4, which showed significant improvement in retinal thickness when transducing progranulin (Figure 5D). The result suggests that earlier treatment not only led to improvement in lysosomal function, but it also reduced photoreceptor cell death. Whether this owes to early or systemic delivery is unknown. Intravenous delivery of the viral load likely led to progranulin expression in other organs, resulting possibly in systemic immune tolerance. While it has been shown that systemic injections with AAV9 in neonatal mice leads to the production of anti-AAV9 antibodies, another study has reported that systemic delivery to neonatal mice (P2) does not lead to the production of antibodies against their transduced protein of interest (factor VIII protein expressed in mice that model hemophilia A).[29,30] The analysis of an immune response specific to PGRN is necessary, as the identification of an adaptive immune response to the protein after systemic and intravitreal delivery warrants further study. Moreover, the question of

Table 2. AAV viral titers established through qPCR

rAAV (100–150 μL)	Titer (vg/mL)
7m8-scCAG-mPGRN	3.73E+13
7m8-scCAG-mPGRN	3.17E+14
7m8-scCAG-hPGRN	3.0E+12
7m8-scCAG-hPGRN	1.84E+13
AAV92YF-scCAG-mPGRN	1.20E+14
AAV92YF-scCAG-hPGRN	1.10E+14

clinical translatability arises when retinal thickness improvement was only seen after systemic delivery in neonates. Nevertheless, the results suggest that progranulin delivery and expression under specific circumstances rescue retinal cells.

Interestingly, immunohistochemistry revealed the variability of PGRN expression in retinas of different littermates injected with the same viral aliquot by the same researcher. Importantly, also note that only intracellular progranulin was evidenced by immunolabeling. Extracellular progranulin secreted by infected cells was not analyzed in this study. Furthermore, immunohistochemistry results showed fewer microglial infiltration events in retinas transducing PGRN after injections at 6 and 12 months (Figures 2C, 2D, 2G, 2H, 2K, 2L, 4G, and 4H). These results corroborated previous reports of increases in activated microglia in the hippocampus of $PGRN^{-/-}$ mice.[31] The results also indicated that delivery of PGRN potentially minimized microglial activation in the retina. Further exploration of microglial activation in retinas expressing PGRN is warranted. Moreover, human PGRN did not seem to colocalize with LAMP1, a lysosomal transmembrane protein and marker. Limited puncta in RGCs (Figure 2I) were the only exception reported in this study. What the correct lysosomal localization of transduced PGRN is in neurons remains unanswered. Importantly, also note that hPGRN did not prove to be more toxic than mPGRN when delivered to $PGRN^{-/-}$ mice either intravitreally or intravenously.

In the 2018 study by Arrant et al.,[23] 10- to 12-month-old $PGRN^{-/-}$ mice were stereotaxically injected with rAAV2-CBA-mPGRN in the mPFC and showed reduction in microgliosis and lipofuscin accumulatioin in different brain regions. They demonstrated an improvement in lysosomal function by the analysis of cathepsin D expression and LAMP1. Most curiously, they also indicated that $PGRN^{-/-}$ mice mount a strong local immune response to transduced PGRN, associated with a higher antibody production than compared to mice injected with rAAV2-CBA-GFP.

In a later study, Amado et al.[24] examined histologically the brains of $PGRN^{-/-}$ mice transducing progranulin. Stereotaxic injections of rAAV4-CAG-hPGRN or rAAV9-CMV-hPGRN in the posterior right lateral ventricle of 6- to 8-month-old $PGRN^{-/-}$ mice led to atrophy of the hippocampus, linked to toxic CD4 T-cell infiltration. Interestingly, animals injected with AAV9-CMV-GFP or AAV4-CAG-GFP did not exhibit the same level of hippocampal damage or cellular infiltrate as did injection with AAV9-CMV-hPGRN or AAV4-CAG-hPGRN, indicating that degeneration occurred because of transduction of progranulin and not as a response to the viral capsid. They also reported an increase in microgliosis and astrogliosis in the hemisphere transducing PGRN, hence suggesting that progranulin, while capable of improving lysosomal function and reducing lipofuscin deposits, may exacerbate cell loss when delivered to adult $PGRN^{-/-}$animals.

The retinal changes in response to progranulin transduction observed in our study seemed to fall in line with observations in the Arrant et al.[23] and Amado et al.[24] studies. We observed a strong reduction in lipofuscin accumulation and a clear decrease in microgliosis. However, there was a noticeable lessening in retina thickness and photoreceptor nuclei in injected adult animals. Importantly, also note the differences in cell targeting by 7m8 and AAV9.2YF; the former only offers PGRN transduction in the retina, and the latter results in systemic expression of PGRN. An immune response to PGRN is one possible explanation. $PGRN^{-/-}$ mice are known to present an exacerbated inflammatory response to injury or stressors, which can be a contributing factor to the results observed.[31–33] While it has not been confirmed that transduced PGRN was released to the extracellular space, it is possible that $PGRN^{-/-}$ mice mounted an immune response to this extracellular protein when exposed to it later in life. The delivery of PGRN to P3–P4 mice is consistent with this explanation, as mice systemically exposed to the protein from an early age might not mount an immune response to it. More comprehensive studies of systemically treated $PGRN^{-/-}$ pups are warranted, as well as studies to specifically investigate the possibility of an immune response against PGRN in animals treated at an older age. Correct shuttling of transduced PGRN, delivered via AAV, is also unknown. While immunohistochemistry for PGRN in our study points toward vesicular localization, this finding requires confirmation. Nevertheless, the positive outcomes for mice injected at an early age, such as reduction in lipofuscinosis and microgliosis, and an increase in retinal thickness, are promising. The effect of PGRN gene therapy in the retina serves as a proof of point for further investigating PGRN gene therapy in PGRN-related NCL disease.

MATERIALS AND METHODS

Production of viral vectors

rAAV was packaged in HEK293T cells by transient plasmid co-transfection as previously described.[34] The capsid serotype plasmids were 7m8 or AAV9.2YF Rep/Cap, scCAG-mPGRN or scCAG-hPGRN was used as the transgene, and an adenovirus (Ad) helper plasmid was used in all preparations.[34] The virus was purified with iodixanol ultracentrifugation gradient, and buffers exchanged with Amicon Ultra-15 centrifugal filter units, so the final viral stock was in sterile PBS. Viral titers were established via qPCR, with primers for inverted terminal repeats (ITRs) (Table 2).

Animals and injections

The experiments were authorized by the Animal Care and Use Committee, Office of Animal Care and Use at UC Berkeley (AUP 2014-09-6705). All experiments were conducted according to The Association

Table 3. Animal cohorts showing the age at which each one was injected, method of injection, viral construct, and age when animals were euthanized

Age at injection	Method	Viral construct	Age at euthanasia
1 month	intravitreal	AAV2.7m8-scCAG-mPGRN	12 months
6 months	intravitreal	AAV2.7m8-scCAG-mPGRN	12 months
		AAV2.7m8-scCAG-hPGRN	
12 months	intravitreal	AAV2.7m8-scCAG-mPGRN	18 months
Post-natal day 3 or 4	systemic	AAV9.2YF-scCAG-mPGRN	12 months
		AAV9.2YF-scCAG-hPGRN	

Table 4. Antibodies and their dilutions

Antibody	Company	Dilution
Sheep anti-mPGRN	R&D Systems (Minneapolis, MN, USA), AF2557	1:500
Goat anti-hPGRN	R&D Systems, AF2420	1:500
Rabbit anti-IBA1	Fujifilm Wako Diagnostics (Mountain View, CA, USA), 019-19741	1:1,000
Rabbit anti-LAMP1	Abcam (Cambridge, UK), ab24170	1:1,000
Alexa Fluor 488 anti-goat	Thermo Fisher Scientific (Waltham, MA, USA), A32814	1:2,000
Alexa Fluor 594 anti-sheep	Thermo Fisher Scientific, A11016	1:2,000
Alexa Fluor 594 anti-rabbit	Thermo Fisher Scientific, A21207	1:2,000

for Research in Vision and Ophthalmology (ARVO) Statement for the Use of Animals and the guidelines of the Office of Laboratory Animal Care at UC California Berkeley. $PGRN^{+/-}$ mice were obtained from the Gladstone Institute at UCSF, as originally described by Martens et al.[17] Initially, $PGRN^{+/-}$ mice were backcrossed into C57BL/6J mice, and then $PGRN^{-/-}$ breeding pairs were set up. All mice were housed at a 12-h light/12-h dark cycle with *ad libitum* access to food and water. For intravitreal injections, mice were anesthetized with intraperitoneal injections of ketamine (72 mg/kg) and xylazine (64 mg/kg). To enter the vitreous chamber, the sclera was punctured posterior to the limbus with a disposable $30^1/_2$G needle. A blunt needle attached to a glass Hamilton syringe was used to deliver 2 μL of AAV via the same path into the vitreous cavity, over the optic nerve head. Contralateral control eyes were injected with 2 μL of sterile PBS. The tail vein was used in pups for intravenous injections, where 10 μL of viral stock was delivered using sterile BD Ultra-Fine (31G) insulin syringes. Corresponding injected viral titers can be found in Table 2. Injection time points, along with viral constructs, can be found in Table 3.

ERG recording

Mice were dark adapted overnight in dark boxes, and ERGs were performed between 8:30 a.m. and 12:30 p.m. Mice were anesthetized with intraperitoneal injections of ketamine and xylazine as aforementioned, and one drop of tropicamide (1%) and phenylephrine (2.5%) each was applied topically for pupil dilation. Mice were then positioned on a heated platform and contact lens recording electrodes were placed on corneas of both eyes, with a ground electrode inserted subcutaneously between both eyes, and a reference electrode was introduced subcutaneously in the tail. Scotopic ERGs were first recorded as three flashes at 1 log cd × s/m^2 on a dark background and averaged. Rod responses were then saturated by a bright background for 5 min. Second, photopic responses were recorded at 1.4 log cd × s/m^2 and presented on a light background. ERGs were recorded with an Espion E2 system (Diagnosys, Lowell, MA, USA) and data were analyzed with MATLAB (MathWorks, Natick, MA, USA) to extract A and B wave amplitudes from recordings.

OCT

Retinal images were captured *in vivo* using an 840 nm SDOIS OCT system (Bioptigen, Durham, NC, USA) including an 840 nm SDOIS engine with a 93-nm bandwidth internal source providing a tissue resolution of less than 3.0 μm. Animals were anesthetized with intraperitoneal injections of ketamine and xylazine, and pupils were dilated with tropicamide and phenylephrine, as previously described. Superior and inferior retinal hemispheres were imaged in 96 sections, which were averaged into eight slices. The thickness of the total retina, from the ILM to the RPE, and photoreceptor layers, from the ONL to the RPE, were measured with InVivoVue software (Bioptigen, Durham, NC, USA) and Fiji (Fiji is essentially ImageJ, National Institutes of Health, Bethesda, MD, USA) from the superior and inferior sections that showed the optic nerve head.[35]

Immunohistochemistry

Mice were euthanized with a CO_2 overdose and cervical dislocation. Eyes were enucleated and fixed in paraformaldehyde (4%) overnight, then washed in PBS. Eyes were dissected, the cornea, lens, and vitreous were removed, and the remaining eye cups were incubated in 30% sucrose overnight. Eye cups were then embedded in optimal cutting temperature (O.C.T.) compound and sectioned with a Leica CM3050 cryostat (Leica Biosystems, Buffalo Grove, IL, USA). Retinal sections were washed with PBS, incubated with Triton X-100 (0.5%) and BSA (1%) for 15 min, then BSA (1%) for 1 h. Sections were incubated overnight with primary antibodies (Table 4) in BSA 1%. On the following day slides were washed three times with PBS, then incubated with secondary antibodies (Table 4) in BSA (1%) for 1 h at room temperature. After two PBS washes, sections were mounted with Vectashield antifade mounting medium with DAPI. Slides were imaged with a laser scanning confocal microscope (LSM 710, Carl Zeiss, Oberkochen, Germany).

Lipofuscin imaging and quantification

After sectioning, retinas were incubated with Triton X-100 (0.5%) and BSA (1%) for 15 min, washed with PBS, and mounted with Vectashield antifade mounting medium and DAPI. All sections used for lipofuscin quantification were centered on the optic nerve. Sections were imaged with either a 488- or 564-nm laser with the same settings. Images were processed with Fiji, then transformed into binary images and particles were counted. Total area covered by autofluorescent particles was divided by the total area covered by DAPI and

multiplied by 100. ONL nuclei were quantified over 200 μm using cross-section images obtained for lipofuscin quantification.

Statistical analysis

A two-way ANOVA with multiple comparisons was performed for OCT and ERG measurements between experimental groups, with the Geisser-Greenhouse correction and Fisher's least significance difference (LSD) test. A Mann-Whitney statistical test (non-paired) or Wilcoxon signed rank test (paired) was performed for lipofuscin or ONL quantification. In OCT and ERG graphs, symbols represent means and error bars represent ± standard deviation. In box-and-whiskers plots, boxes show the interquartile range (25%–75%), whiskers represent minimum and maximum values, and horizontal lines represent median values. A p value of less than 0.05 was considered statistically significant and is either indicated with an asterisk or the p value itself. Analysis was performed with GraphPad Prism 9 (GraphPad, San Diego, CA, USA).

SUPPLEMENTAL INFORMATION

Supplemental information can be found online at https://doi.org/10.1016/j.omtm.2021.05.009.

ACKNOWLEDGMENTS

The research was supported by Foundation Fighting Blindness grant TA-GT-0818-0745-UCB. The authors would like to thank Michael Ward and Ari Green at UCSF for supplying the original mouse breeding pairs, Mei Li for helping with viral preparations, Cameron Baker with manuscript editing, and the CNR Biological Imaging Facility, UC Berkeley. Research reported in this publication was supported in part by the National Institutes of Health S10 program under award number 1S10RR026866-01. The content is solely the responsibility of the authors and does not necessarily represent the official views of the National Institutes of Health. The graphical abstract was created using BioRender.

AUTHOR CONTRIBUTIONS

Conceived and designed the experiments, E.A.Z., M.K., and J.G.F.; performed the experiments, E.A.Z., M.V., M.K., D.H., J.T., N.M.-W.; analyzed the data, E.A.Z., D.H., J.T., N.M.-W., and J.G.F.; and wrote the manuscript, E.A.Z. and J.G.F.

DECLARATION OF INTERESTS

The authors declare no competing interests.

REFERENCES

1. Haltia, M. (2006). The neuronal ceroid-lipofuscinoses: From past to present. Biochim. Biophys. Acta *1762*, 850–856.
2. Radke, J., Stenzel, W., and Goebel, H.H. (2015). Human NCL neuropathology. Biochim. Biophys. Acta *1852* (10 Pt B), 2262–2266.
3. Mole, S.E., and Cotman, S.L. (2015). Genetics of the neuronal ceroid lipofuscinoses (Batten disease). Biochim. Biophys. Acta *1852* (10 Pt B), 2237–2241.
4. Smith, K.R., Damiano, J., Franceschetti, S., Carpenter, S., Canafoglia, L., Morbin, M., Rossi, G., Pareyson, D., Mole, S.E., Staropoli, J.F., et al. (2012). Strikingly different clinicopathological phenotypes determined by progranulin-mutation dosage. Am. J. Hum. Genet. *90*, 1102–1107.
5. Huin, V., Barbier, M., Bottani, A., Lobrinus, J.A., Clot, F., Lamari, F., Chat, L., Rucheton, B., Fluchère, F., Auvin, S., et al. (2020). Homozygous GRN mutations: New phenotypes and new insights into pathological and molecular mechanisms. Brain *143*, 303–319.
6. Pottier, C., Ravenscroft, T.A., Sanchez-Contreras, M., and Rademakers, R. (2016). Genetics of FTLD: Overview and what else we can expect from genetic studies. J. Neurochem. *138* (*Suppl 1*), 32–53.
7. Baker, M., Mackenzie, I.R., Pickering-Brown, S.M., Gass, J., Rademakers, R., Lindholm, C., Snowden, J., Adamson, J., Sadovnick, A.D., Rollinson, S., et al. (2006). Mutations in progranulin cause tau-negative frontotemporal dementia linked to chromosome 17. Nature *442*, 916–919.
8. Cenik, B., Sephton, C.F., Kutluk Cenik, B., Herz, J., and Yu, G. (2012). Progranulin: A proteolytically processed protein at the crossroads of inflammation and neurodegeneration. J. Biol. Chem. *287*, 32298–32306.
9. Petkau, T.L., and Leavitt, B.R. (2014). Progranulin in neurodegenerative disease. Trends Neurosci. *37*, 388–398.
10. Zhou, X., Sun, L., Bastos de Oliveira, F., Qi, X., Brown, W.J., Smolka, M.B., Sun, Y., and Hu, F. (2015). Prosaposin facilitates sortilin-independent lysosomal trafficking of progranulin. J. Cell Biol. *210*, 991–1002.
11. Lee, C.W., Stankowski, J.N., Chew, J., Cook, C.N., Lam, Y.-W., Almeida, S., Carlomagno, Y., Lau, K.-F., Prudencio, M., Gao, F.-B., et al. (2017). The lysosomal protein cathepsin L is a progranulin protease. Mol. Neurodegener. *12*, 55.
12. Tanaka, Y., Suzuki, G., Matsuwaki, T., Hosokawa, M., Serrano, G., Beach, T.G., Yamanouchi, K., Hasegawa, M., and Nishihara, M. (2017). Progranulin regulates lysosomal function and biogenesis through acidification of lysosomes. Hum. Mol. Genet. *26*, 969–988.
13. Seehafer, S.S., and Pearce, D.A. (2006). You say lipofuscin, we say ceroid: Defining autofluorescent storage material. Neurobiol. Aging *27*, 576–588.
14. Ahmed, Z., Sheng, H., Xu, Y.-F., Lin, W.-L., Innes, A.E., Gass, J., Yu, X., Wuertzer, C.A., Hou, H., Chiba, S., et al. (2010). Accelerated lipofuscinosis and ubiquitination in granulin knockout mice suggest a role for progranulin in successful aging. Am. J. Pathol. *177*, 311–324.
15. Kayasuga, Y., Chiba, S., Suzuki, M., Kikusui, T., Matsuwaki, T., Yamanouchi, K., Kotaki, H., Horai, R., Iwakura, Y., and Nishihara, M. (2007). Alteration of behavioural phenotype in mice by targeted disruption of the progranulin gene. Behav. Brain Res. *185*, 110–118.
16. Petkau, T.L., Neal, S.J., Milnerwood, A., Mew, A., Hill, A.M., Orban, P., Gregg, J., Lu, G., Feldman, H.H., Mackenzie, I.R.A., et al. (2012). Synaptic dysfunction in progranulin-deficient mice. Neurobiol. Dis. *45*, 711–722.
17. Martens, L.H., Zhang, J., Barmada, S.J., Zhou, P., Kamiya, S., Sun, B., Min, S.-W., Gan, L., Finkbeiner, S., Huang, E.J., and Farese, R.V., Jr. (2012). Progranulin deficiency promotes neuroinflammation and neuron loss following toxin-induced injury. J. Clin. Invest. *122*, 3955–3959.
18. Hafler, B., Klein, Z., and Strittmatter, S. (2013). Progranulin mutant mice exhibit accumulation of intraneuronal lipofuscin aggregates in the retina. Invest. Ophthalmol. Vis. Sci. *54*, 6115, https://iovs.arvojournals.org/article.aspx?articleid=2151132.
19. Hafler, B.P., Klein, Z.A., Jimmy Zhou, Z., and Strittmatter, S.M. (2014). Progressive retinal degeneration and accumulation of autofluorescent lipopigments in progranulin deficient mice. Brain Res. *1588*, 168–174.
20. Ward, M.E., Taubes, A., Chen, R., Miller, B.L., Sephton, C.F., Gelfand, J.M., Minami, S., Boscardin, J., Martens, L.H., Seeley, W.W., et al. (2014). Early retinal neurodegeneration and impaired Ran-mediated nuclear import of TDP-43 in progranulin-deficient FTLD. J. Exp. Med. *211*, 1937–1945.
21. Johnson, T.B., White, K.A., Brudvig, J.J., Cain, J.T., Langin, L., Pratt, M.A., Booth, C.D., Timm, D.J., Davis, S.S., Meyerink, B., et al. (2021). AAV9 gene therapy increases lifespan and treats pathological and behavioral abnormalities in a mouse model of CLN8-Batten disease. Mol. Ther. *29*, 162–175.
22. Kleine Holthaus, S.M., Ribeiro, J., Abelleira-Hervas, L., Pearson, R.A., Duran, Y., Georgiadis, A., Sampson, R.D., Rizzi, M., Hoke, J., Maswood, R., et al. (2018). Prevention of photoreceptor cell loss in a *Cln6*^{nclf} mouse model of Batten disease requires *CLN6* gene transfer to bipolar cells. Mol. Ther. *26*, 1343–1353.

23. Arrant, A.E., Onyilo, V.C., Unger, D.E., and Roberson, E.D. (2018). Progranulin gene therapy improves lysosomal dysfunction and microglial pathology associated with frontotemporal dementia and neuronal ceroid lipofuscinosis. J. Neurosci. *38*, 2341–2358.

24. Amado, D.A., Rieders, J.M., Diatta, F., Hernandez-Con, P., Singer, A., Mak, J.T., Zhang, J., Lancaster, E., Davidson, B.L., and Chen-Plotkin, A.S. (2019). AAV-mediated progranulin delivery to a mouse model of progranulin deficiency causes T cell-mediated toxicity. Mol. Ther. *27*, 465–478.

25. Dalkara, D., Byrne, L.C., Klimczak, R.R., Visel, M., Yin, L., Merigan, W.H., Flannery, J.G., and Schaffer, D.V. (2013). In vivo-directed evolution of a new adeno-associated virus for therapeutic outer retinal gene delivery from the vitreous. Sci. Transl. Med. *5*, 189ra76.

26. Byrne, L.C., Lin, Y.J., Lee, T., Schaffer, D.V., and Flannery, J.G. (2015). The expression pattern of systemically injected AAV9 in the developing mouse retina is determined by age. Mol. Ther. *23*, 290–296.

27. Ward, M.E., Chen, R., Huang, H.-Y., Ludwig, C., Telpoukhovskaia, M., Taubes, A., Boudin, H., Minami, S.S., Reichert, M., Albrecht, P., et al. (2017). Individuals with progranulin haploinsufficiency exhibit features of neuronal ceroid lipofuscinosis. Sci. Transl. Med. *9*, aah5642.

28. Dalkara, D., Byrne, L.C., Lee, T., Hoffmann, N.V., Schaffer, D.V., and Flannery, J.G. (2012). Enhanced gene delivery to the neonatal retina through systemic administration of tyrosine-mutated AAV9. Gene Ther. *19*, 176–181.

29. Zhao, P., Tassew, G.B., Lee, J.Y., Oskouian, B., Muñoz, D.P., Hodgin, J.B., Watson, G.L., Tang, F., Wang, J.-Y., Luo, J., et al. (2021). Efficacy of AAV9-mediated *SGPL1* gene transfer in a mouse model of S1P lyase insufficiency syndrome. JCI Insight *6*, e145936.

30. Hu, C., and Lipshutz, G.S. (2012). AAV-based neonatal gene therapy for hemophilia A: Long-term correction and avoidance of immune responses in mice. Gene Ther. *19*, 1166–1176.

31. Ma, Y., Matsuwaki, T., Yamanouchi, K., and Nishihara, M. (2017). Involvement of progranulin in modulating neuroinflammatory responses but not neurogenesis in the hippocampus of aged mice. Exp. Gerontol. *95*, 1–8.

32. Tanaka, Y., Matsuwaki, T., Yamanouchi, K., and Nishihara, M. (2013). Exacerbated inflammatory responses related to activated microglia after traumatic brain injury in progranulin-deficient mice. Neuroscience *231*, 49–60.

33. Tanaka, Y., Matsuwaki, T., Yamanouchi, K., and Nishihara, M. (2013). Increased lysosomal biogenesis in activated microglia and exacerbated neuronal damage after traumatic brain injury in progranulin-deficient mice. Neuroscience *250*, 8–19.

34. Flannery, J.G., and Visel, M. (2013). Adeno-associated viral vectors for gene therapy of inherited retinal degenerations. Methods Mol. Biol. *935*, 351–369.

35. Schindelin, J., Arganda-Carreras, I., Frise, E., Kaynig, V., Longair, M., Pietzsch, T., Preibisch, S., Rueden, C., Saalfeld, S., Schmid, B., et al. (2012). Fiji: an open-source platform for biological-image analysis. Nat. Methods *9*, 676–682.